IEEE Access
Multidisciplinary | Rapid Review | Open Access Journal

Received October 24, 2019, accepted November 14, 2019, date of publication December 9, 2019, date of current version February 11, 2020.

Digital Object Identifier 10.1109/ACCESS.2019.2958390

Miniaturized Dual-Band Bandpass Filter With Sharp Roll-Off Using Ring-Loaded Resonator

DAOTONG LI[1], (Member, IEEE), JU-AN WANG[1,2,3], YING LIU[1], AND ZHEN CHEN[1,3]

[1]Center of Communication and Tracking Telemetry Command, Chongqing University, Chongqing 400044, China
[2]State Key Laboratory of Millimeter Waves, Nanjing 210096, China
[3]School of Microelectronics and Communication Engineering, Chongqing University, Chongqing 400044, China

Corresponding author: Daotong Li (dli@cqu.edu.cn)

This work was supported in part by the National Natural Science Foundation of China under Grant 61801059, in part by the graduate research and innovation foundation of Chongqing under Grant CYS19062 and Grant CYS19057, in part by the Opening Fund of State Key Laboratory of Millimeter Waves under Grant K202016, in part by the Basic Research and Frontier Exploration Special of Chongqing Natural Science Foundation under Grant cstc2019jcyj-msxmX0350, and in part by the Chongqing Special Found of Technology Research and Development for Academician under Grant cstc2018zdcy-yszxX0001.

ABSTRACT In this paper, a miniaturized dual-band bandpass filter (BPF) with good selectivity based on ring-loaded resonator (RLR) and 0° feed structure is proposed. First, the RLR is investigated theoretically and numerically, and a miniaturized Filter I is designed based on the RLR and filter synthesis approach. Secondly, based on the coupling structure of the previous BPF and theory of 0° feed structure, the sub Filter II is formed. By appropriately adjusting the location of the I/O ports, the dual-band filter can be achieved simply. The proposed dual-band BPF provides compact size and satisfactory out-of-band rejection between each band with multiple transmission zeros (TZs) introduced by source/load coupling and a special coupling scheme.

INDEX TERMS Bandpass filter, compact, dual-band, 0° feed structure, ring-loaded resonator.

I. INTRODUCTION

As one of the key components of modern multiservice wireless communication systems, the behavior of the bandpass filters (BPFs) influences greatly the performance of the whole system [1]–[3]. Therefore, dual-band bandpass filters (BPFs) with excellent frequency responses, such as compact size, good isolation, sharp roll-off skirt, and undistorted passband [4]–[8], are desired.

To meet the requirement, much research work has been performed and various design approaches have been proposed. Among them, two categories of methods are very popular. The first category is to utilize a resonator's fundamental and second harmonic frequencies to form dual-band BPF [9]–[13]. A typical case is to employ stepped impedance resonators (SIRs). In [9], [10], trisection hairpin resonator, and modified SIR are proposed and used to realized dual-band BPF design. In [11], a compact dual-band interdigital BPF has been reported based on the hybrid resonators with series and shunt resonances. The first two resonant frequencies of these resonators are controlled to build up a dual-band bandpass response. In [12], [13], dual-band BPFs based on dual-mode SIRs have been proposed. By controlling impedance and length ratios of SIRs, desired operating frequencies are obtained. However, it is not convenient to meet specific bandwidth requirement. The second category is to utilize multi-mode resonator (MMR). For example, some dual-mode resonators like open/short stub-loaded SIRs [14], open/short-circuited stub-loaded $\lambda/4$ resonators [15] and dual-mode SLRs and SIRs [14], [16] are employed to design dual-band BPFs, respectively. Besides, for reducing filter size and improving the passband selectivity, quad-mode resonators, such as single quad-mode SLRs [17]–[19], are used to realize dual-band filter designs. Here, the first two resonance modes are utilized to form the lower passband, while the third and fourth resonance modes form the higher passband. However, the appropriate coupling between the resonant modes of these resonators should be carefully tuned to get a dual-band BPF. In [20], two high temperature superconducting dual-band BPFs based on quint-mode stub-loaded resonator have been proposed. The quint-mode resonator is constructed by loading four open stubs in shunt.

Since the ring resonator owns the advantages of compact size and high-quality (Q) factor, it is widely used to excite resonant modes in the other kinds of MMR-based BPFs [21]–[26]. The BPF with an adjustable bandwidth in the

The associate editor coordinating the review of this manuscript and approving it for publication was Qingfeng Zhang.

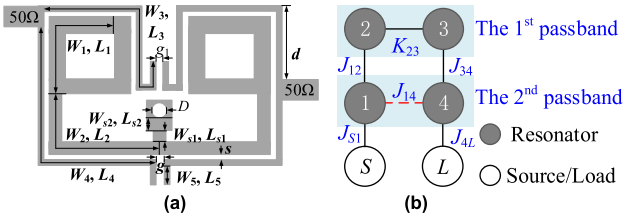

FIGURE 1. The proposed dual-band BPF, (a) the structure of proposed dual-band BPF, (b) the coupling diagram.

second-passband is realized by using a stepped impedance ring resonator [21]. However, only one transmission pole (TP) could be generated in the second passband. To improve the performance of the dual-band BPF with ring resonators, four resonant modes are excited in the BPFs of [22]–[25]. Degenerate modes as well as multiple transmission zeros (TZs) created by loading parallel-coupled lines [22], [23], shorted stubs [24] and open-circuited stubs [25] on the ring resonator are proposed to achieve dual-band performances. In addition, high temperature superconductor was used to fabricate MMR-based BPFs with low loss and compact size [26]. However, the passband of the ring resonator-based BPFs of [21]–[26] is either narrow or unadjustable since the degrees of freedom of the filter parameters are limited. Up till now, dual-band BPF with controllable bandwidths was only presented in [27], [28]. Nevertheless, the bandwidths of the two passbands are not wide enough for many wireless communication systems.

In this paper, a miniaturized dual-band BPF structure designed using a conventional uniplanar printed circuit board (PCB) process, as shown in Fig. 1, is proposed, which not only has the controllable bandwidth and frequency space, but also achieves a wide stopband. First, a miniaturized BPF (Filter I) is designed based on the ring-loaded resonator and filter synthesis approach. Based on the coupling structure of the Filter I and theory of 0° feed structure, the second passband is formed. By appropriately adjusting the location of the I/O ports, the dual-band filter can be achieved simply. The 0° feed structure is employed not only to generate one of the passbands, but also to feed other resonators to form the other passband. The proposed dual-band BPF provides compact size and satisfactory out-of-band rejection between each band with multiple transmission zeros (TZs) introduced by source/load coupling and a special coupling scheme. Using the proposed design method, the required external quality factors and coupling coefficients can be obtained at two passbands. It is easy to meet performance requirements of two passbands, i.e., center frequencies and bandwidth.

The design procedure is organized as follows. In Section II, the design principles of the dual-band are introduced. The approaches for the first and second sub passbands are described in Section II-A and B, respectively, and Section II-C gives the design and analysis of the combination of the dual-band BPF. In Section III, a fabricated

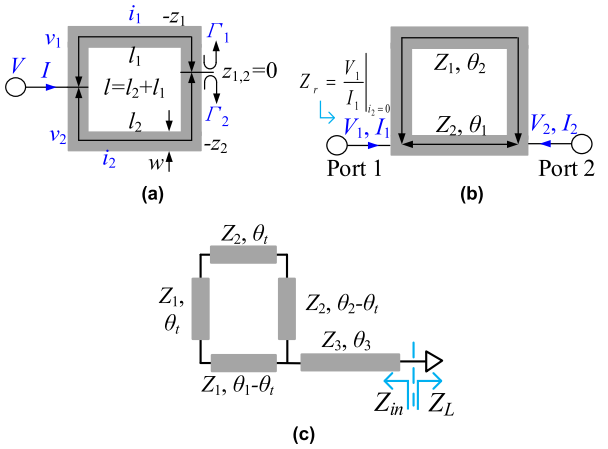

FIGURE 2. Ring-loaded resonator, (a) one-port ring resonator, (b) two ports ring resonator, (c) The structure proposed RLR.

dual-band BPF with central frequencies of 2.4/5.2 GHz and fractional bandwidths of 21/11.5% is presented. Some conclusions are drawn in Section IV. All the analyses and simulations are carried out by using full-wave EM simulator Ansys HFSS and Advanced Design System (ADS), and the filters design and fabrication are implemented on the substrate *Taconic* RF-35 ($\varepsilon_r = 3.5$, $\mu_r = 1.0$, $\tan\delta = 0.0018$ and $h = 0.508$ mm).

II. DESIGN OF FILTER I

A. THEORY OF RING-LOADED RESONATOR

According to the [29], a simple transmission-line model unaffected by boundary conditions can be used to calculate the resonant frequencies of ring resonators. Fig. 2(a) shows the structure of the one-port square ring resonators. The total length l can be divided into l_1 and l_2 transmission line sections. z_1 and z_2 are the coordinates corresponding to sections l_1 and l_2, respectively. Thus, it can be investigated by viewing it as a microstrip line that ends on itself, and its equivalent circuit is shown in Fig. 2(b). With both ends of the two split sections connected, port 1 is used to designate the feeding port and port 2 is arbitrarily chosen and kept open-circuited outside, since there is nothing connected there. The ring is fed by the voltage source V at somewhere with $z_{1,2} < 0$. The positions of the zero point of $z_{1,2}$ and the voltage V are arbitrarily chosen on the ring. According to the transmission line theory [29]–[31], the input impedance of a one-port ring resonator can be derived. The ABCD transfer matrices for the individual sections can be given as follows

$$\begin{bmatrix} A & B \\ C & D \end{bmatrix}_i = \begin{bmatrix} \cos\theta_i & jZ_i \sin\theta_i \\ jY_i \csc h\theta_i & \cos\theta_i \end{bmatrix}, \quad i = 1, 2. \quad (1)$$

where θ_i and $Z_i = 1/Y_i$ ($i = 1, 2.$) are the electrical length and impedance of the transmission lines sections, respectively. The Y admittance matrices for the upper and lower section can be further obtained from the ABCD matrices by

performing the matrix transformation [31]

$$\begin{aligned}\begin{bmatrix} Y_{11} & Y_{12} \\ Y_{21} & Y_{22} \end{bmatrix}_{ring} &= \begin{bmatrix} Y_{11} & Y_{12} \\ Y_{21} & Y_{22} \end{bmatrix}_{upper} + \begin{bmatrix} Y_{11} & Y_{12} \\ Y_{21} & Y_{22} \end{bmatrix}_{lower} \\ &= j\begin{bmatrix} -Y_1\cot\theta_1 & Y_1\csc\theta_1 \\ Y_1\csc\theta_1 & -Y_1\cot\theta_1 \end{bmatrix} \\ &\quad + j\begin{bmatrix} -Y_2\cot\theta_2 & Y_2\csc\theta_2 \\ Y_2\csc\theta_2 & -Y_2\cot\theta_2 \end{bmatrix} \end{aligned} \tag{2}$$

Thus, when $Z_1 = Z_2 = Z_0$, the input impedance of the one-port ring resonator can be obtained as

$$Z_r = \frac{V_1}{I_1}\bigg|_{I_2=0} = \frac{Y_{22}}{Y_{11}Y_{22}-Y_{12}Y_{21}} = -j\frac{Z_0}{2}\frac{\sin(\theta_1+\theta_2)}{1-\cos(\theta_1+\theta_2)}. \tag{3}$$

Based on the one-port ring resonator, a novel resonator is proposed, which is shown in Fig. 2(c). It consists of a transmission line section with impedance Z_3 and electrical length θ_3, and the loaded one-port ring structure, which is called as ring-loaded resonator (RLR). The right-end of Z_3 section is short-circuited, and thus $Z_L = 0$. For analysis simplicity, $Z_1 = Z_2 = Z_3 = Z_0$ is assumed in this work, and the impedance Z_{in}, as indicated in Fig. 2(c), is deduced as

$$Z_{in} = jZ_0\frac{2\tan\theta_3\,(1-\cos(\theta_1+\theta_2)) - \sin(\theta_1+\theta_2)}{2\,(1-\cos(\theta_1+\theta_2)) + \sin(\theta_1+\theta_2)\tan\theta_3}. \tag{4}$$

Under the transversal resonant conditions, the proposed RLR satisfies $Z_{in} + Z_L = 0$, and the fundamental and first spurious frequencies can be derived from

$$2\tan\theta_3\,(1-\cos(\theta_1+\theta_2)) - \sin(\theta_1+\theta_2) = 0 \tag{5}$$

and the reactance slope x of RLR can be deduced as

$$x_{in} = \frac{f}{2}\frac{dX_{in}}{df}\bigg|_{f=f_0}. \tag{6}$$

However, the line dispersion and the parasitic effects of discontinuities also impact the exact locations of the frequencies of these transmission poles. As described in Ref. [25], when the transmission line length θ_3 on the ring resonator length increases, all the transmission pole frequencies become smaller. To further explore the resonant characteristics of the proposed RLR shown in Fig. 2(c), as an example, θ_2 and θ_3 are set as 30° and 30°, respectively. All the electrical lengths are in respect to the fundamental frequency of 2.4 GHz and the characteristic impedance Z_0 of transmission lines is set to 100 Ohm. Fig. 4 (a) and (b) plot the frequency ratio f_1/f_0 (f_0 is the fundamental resonant frequency, and f_1 is the first spurious resonant frequency) versus the impedance ratio Rz ($Rz = Z_1/Z_2$) and electrical length ratio $\alpha(\alpha = \theta_1/(\theta_1+\theta_2))$, respectively. It is observed from Fig. 4(a) that as the electrical length ratio α becomes larger, the frequency ratio f_1/f_0 increases first and then descends. It is worth noting that the frequency ratio f_1/f_0 reaches the peak values when the electrical length ratio α is 0.75 ($\theta_1 = 90°$). Furthermore, under the condition of $\alpha < 0.75$, the larger the

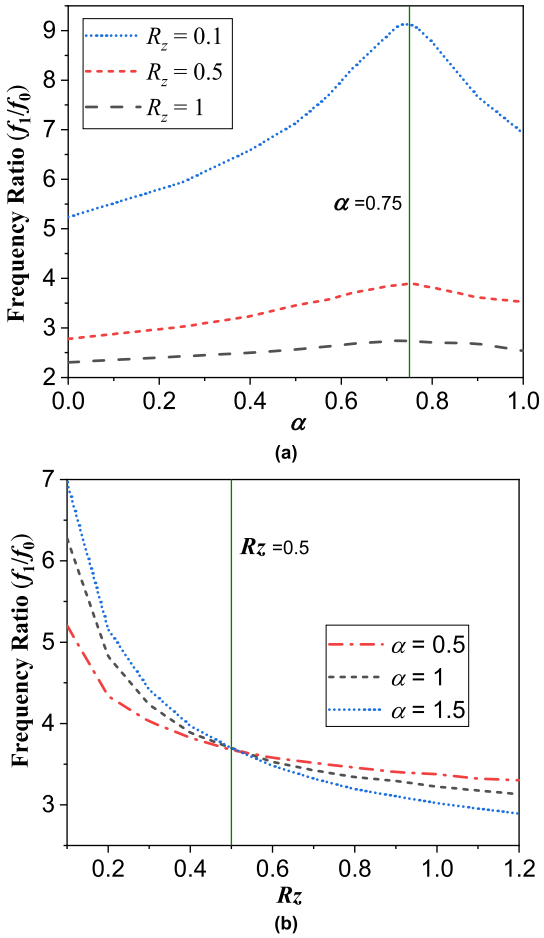

FIGURE 3. Impacts of (a) electrical length ratio α and (b) impedance ratio Rz on the frequency ratio of fundamental and first spurious resonant frequencies (f1/f0), respectively.

impedance ratio Rz, the higher slope of frequency ratio f_1/f_0. That is, as α increases, the frequency ratio f_1/f_0 changes faster and higher frequency ratio f_1/f_0 can be obtained.

Similarly, the impacts of impedance ratio Rz and electrical length ratio α are also numerical investigated, as shown in Fig. 4(b). When the impedance ratio Rz increases, the frequency ratio f_1/f_0 decreases dramatically. Moreover, for the impedance ratio Rz less than 0.5, the larger electrical length ratio α is, the higher frequency ratio f_1/f_0 is. On the contrary, when the impedance ratio Rz is large than 0.5, the frequency ratio f_1/f_0 is higher as the electrical length ratio α decreases.

Therefore, the fundamental and spurious resonant frequencies can be controlled.

B. DESIGN OF FILTER I

Based on the RLR and filter synthesis method [33], a BPF is designed by using the K inverter shown in the inset of Fig. 4(b). The equivalent coupling topology of the proposed dual-band BPF based on RLR in the alternative J-K-J form is shown in Fig. 4(a), in which the J inverters are formed by the asymmetric parallel coupled lines (APCL) section. Fig. 5(a) and (b) display the structure and coupling diagram

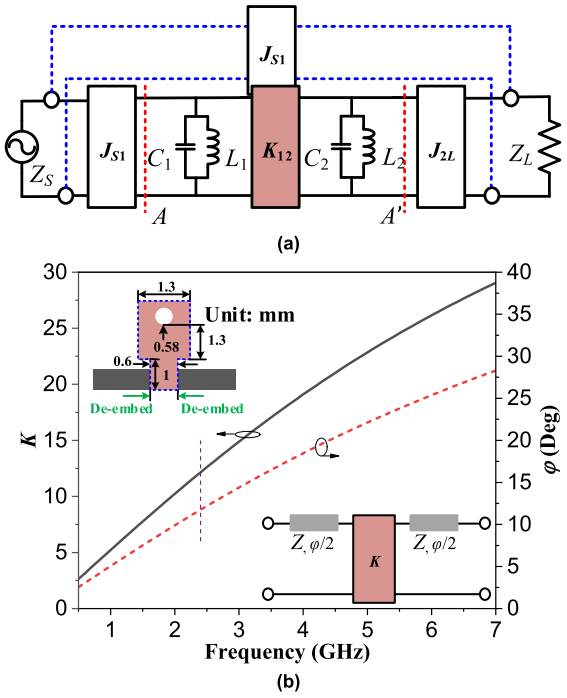

FIGURE 4. Schematic of proposed Filter I and K inverter, (a) schematic of the Filter I, (b) de-embedded value K and associated electrical length as the function of frequency.

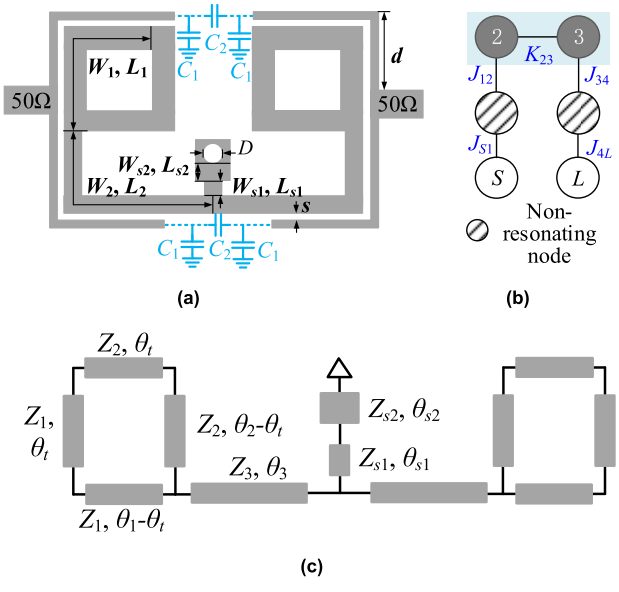

FIGURE 5. Filter I, (a) geometry of proposed Filter I, (b) coupling diagram, (c) structure of resonant element.

of the Filter I, consisting of resonant element, a pair of APCL sections and I/O ports. The APCL sections play the role of coupling, which is non-resonating nodes. Fig. 5(c) shows the corresponding geometry of the resonant element which is composed of a couple of RLRs inductively coupled by K inverter.

We firstly calculate the dimensions of K inverter according to the K inverter design curves shown in Fig. 4(b) and the specifications of desired BPF, and then derive the preliminary dimensions of uncoupled RLRs according to the central frequency f_1 and the reactance slope of x. Finally, by combining the RLRs and K inverter along with the proper coupling structure and I/O ports, the BPF can be achieved.

A 2nd-order Chebyshev BPF centered at $f_0 = 2.4$ GHz with 20-dB in-band return losses, and the fractional bandwidths of $\Delta_1 = 10.6\%$ is designed. Based on the specified central frequencies f_0, the $K = 12.1$ can be derived, and proper parameters of RLR can thus be selected from the Fig. 4(b). It can be observed that when the parameters of the K inverter are selected as $D = 0.58$ mm, $L_{s1} = 2.2$ mm, $L_{s2}2.2$ mm, $W_{s1} = 0.6$ mm, and $W_{s2} = 1.3$ mm, the $K = 12.5$ at the frequencies of 2.4 GHz. Moreover, the associated electrical length is 11.74°, which is equal to physical length of 2.22 mm.

With the central frequency of f_0 and the reactance slope x, the dimensions of RLR can be rigorously derived to meet the specified K couplings at the passband based on the synthesis approach [33]. Therefore, the preliminary dimensions of an uncoupled RLR in Fig. 2(c) can be determined as: $W_1 = 0.8$ mm, $L_1 = 4.15$ mm, $W_2 = 0.3$ mm, $L_2 = 6.55$ mm.

For the APCL segments with physical width (W_3, L_3) and (W_4, L_4), they can be modelled as an admittance inverter. The external quality factors of input and output sections named as the J_{s1} and J_{2L} in Fig. 4(a) can be extracted, and the extraction formula of quality factor [34] is listed as follows:

$$Q_{Ex} = \frac{f_0}{\Delta f_{\pm 90^\circ}} \tag{7}$$

$$\Delta k = \frac{g_0 g_1}{Q_{Ex}} = \frac{g_2 g_3}{Q_{Ex}} \tag{8}$$

where f_0 and $f_{\pm 90^\circ}$ represent the resonant frequency and the fractional bandwidth between the $\pm 90^\circ$ points of S_{11} phase response for the feeding structure related to each band. g_0, g_1, g_2 and g_3 represent the prescribed second order low-pass filter prototype parameters. With prescribed filter responses and equation (7), the impacts of the APCL parameter s on the external quality factor Q_{Ex} for passband is plotted in Fig. 6. The corresponding parameters of the APCL can be determined as shown in the inset of Fig. 6 with the specifications.

Based on the above analysis, the BPF is obtained. The structure and the coupling schematic are shown in Fig. 5(a) and (b), respectively. Since all the realistic effects including impedance steps and all parasitics are taken into consideration in full-wave simulation, the final filter has been fine-tuned, and transmission coefficient are shown in Fig. 7. The passband is centered at 2.4 GHz. It should be noted that there is no transmission zero besides the passband. For improving the passband selectivity and rejection of stopband, source-to-load coupling is introduced by lengthening the length of APCL with the in-band performances unchanged. The final simulated results are also shown in Fig. 7. From the comparison of the BPF with and without source-to-load coupling in Fig. 7, it can be found that the BPF with source-to-load coupling has a higher roll-off and suppression response. Moreover, to further clarify the operating mechanism,

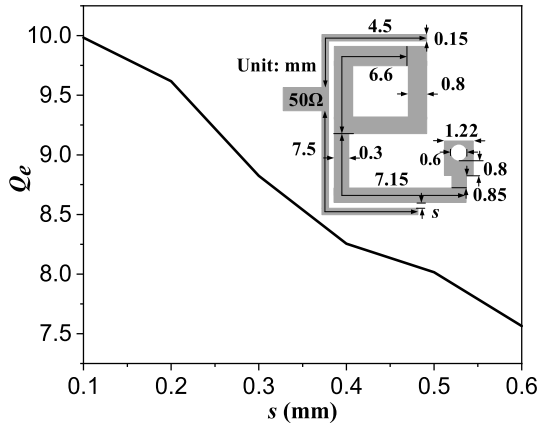

FIGURE 6. Extracted external quality factor of filter I.

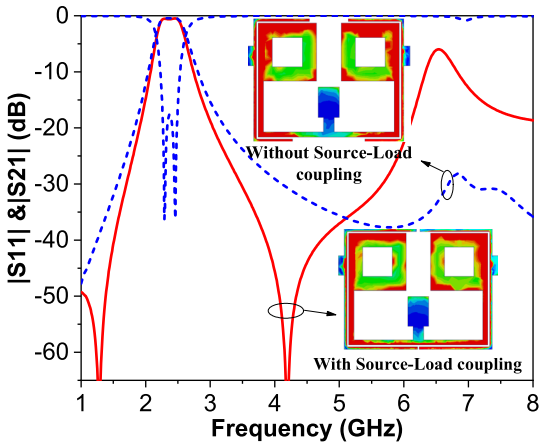

FIGURE 7. Simulated transmission coefficients of filter I with and without source to load coupling. (The insets are simulated electric field distribution in 2.4 GHz.)

the electric field distribution of the filter under the two operating conditions are also shown in the inset of Fig. 7.

III. DESIGN OF FILTER II

Herein, as shown in Fig. 8, a novel Filter II with electric coupling structure is proposed based on electric coupling and the theory of 0° feed structure. The lower and upper paths have the same electric lengths at the fundamental resonant frequency of the split-ring, which has a 0° difference between the electric delays of the lower and upper paths. Moreover, as shown in the inset of Fig. 8, the coupling gaps between the two resonators can be modeled as π-networks, where the values of C_1 and C_2 could be found from [35]. The C_1 will be neglected because the value of ωC_1 is usually small ($C_1 < 0.01$ pF) for a lower microwave frequency range.

According to the Ref. [36], the transmission matrix of the whole Filter II structure can be derived, and the transmission coefficient of Filter II can be found. Furthermore, by using the proposed structure, a pair of transmission zeros at around the cutoff frequencies are introduced to improve the selectivity of the Filter II.

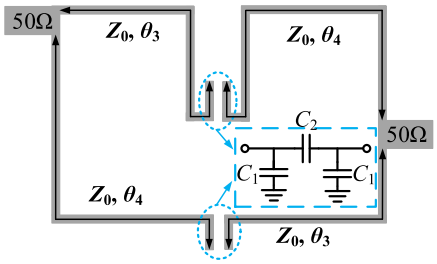

FIGURE 8. Filter II based on electric coupling.

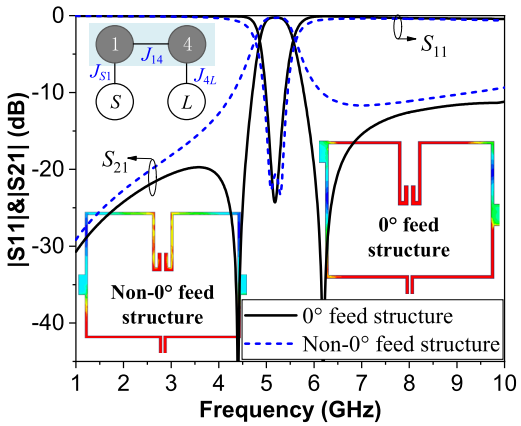

FIGURE 9. Simulated transmission coefficients of filter II with non-0° feed structure and 0° feed structure, respectively. (The insets are simulated electric field distribution in 5.2 GHz.)

Fig. 9 is the comparison of the Filter II with the non-0° feed structure and 0° feed structure at the center frequency 5.2 GHz. When 0° feed structure is applied, $\theta_3 = 89.5°$ and $\theta_4 = 124.2°$ at the center frequency 5.2 GHz. Two zeros are obtained at 4.38 and 6.20 GHz, when θ_3 and θ_4 approach $\pi/2$, respectively, the stopband rejection is greatly increased.

Based upon the previous discussions, the Filter II centered at 5.2 GHz with in-band return loss of 20 dB, and the fractional bandwidths of $\Delta_2 = 13.8\%$ is proposed. The model for Filter II with a 0° feed structure is proposed and shown in Fig. 8. One resonator is resonant at the frequency when θ_3 approaches $\pi/2$ and the other is resonant at the frequency when θ_4 is approximately $\pi/2$. These two zeros are close to the passband and on either side of the passband, therefore, significantly increase the stopband rejection.

IV. DUAL-BAND BPF DESIGN

Based on the analyses of Filter I and II, a dual-band BPF, as shown in Fig. 1(a), is proposed. Fig. 1(b) shows the coupling diagram. By combining the aforesaid Filter-I (2.4 GHz) and Filter-II (5.2 GHz) into one single structure, the dual-band BPF with easier band allocation is realized with a fine adjustment. It can be seen that the proposed dual-band BPF contains a pair of inductively cascaded RLRs and a 0° feed structure, and Fig. 10 shows the simulated transmission coefficients of the sub filter I, sub filter II and the combined dual-band BPF. It is clear that two passbands of the proposed dual-band BPF overlap the passbands of Filter I and Filter II, respectively, and the in-band performances keep almost the

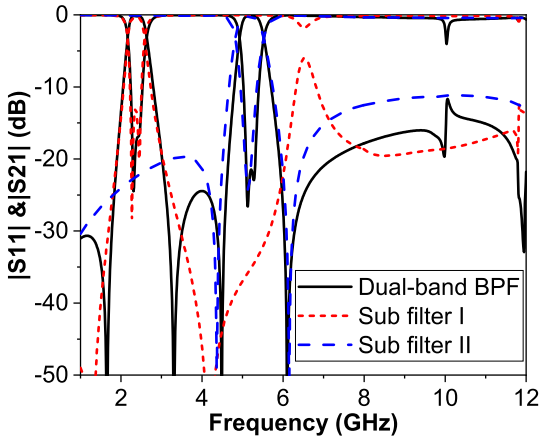

FIGURE 10. EM simulated results of transmission coefficients for the proposed dual-band BPF and sub filters.

TABLE 1. Comparison of some previous dual-band filters.

Ref.	CF (GHz)	FBW (%)	IL (dB)	TZs	Circuits Size ($\lambda_g \times \lambda_g$)
[9]	1.57/2.4	5/2	1/1	0	0.22 × 0.22
[10]	3.45/5.27	10.7/4	1.76/1.76	5	0.23 × 0.31
[11]	0.9/1.3	2.86/3.32	5.1/2.7	1	0.63 × 0.21
[12]	1.68/2.99	3.27/2.85	1/1	3	0.86 × 0.65
[13]	1.5/2.5	10/5	2.13/2.88	0	0.31 × 0.1
[14]	1.63/2.73	7.5/5.1	1.5/2.15	7	0.25 × 0.25
[15]	2.4/5.8	4.63/3.6	1.35/1.97	3	0.39 × 0.25
[16]	1.84/2.9	8.1/6.8	1.7/1.6	3	N.A.
[17]	1.8/3.5	14/10	0.8/0.6	5	0.15 × 0.12
[20]*	1.8/2.4	7.91/3.89	0.08/0.08	3	0.46 × 0.34
[21]	2.4/5.2	6/7	2.5/3.2	3	0.19 × 0.19
[22]	2.38/4.87	6.7/8	2/1.4	4	N.A.
[23]	2.6/5.8	10.4/3.6	1.1/2.15	4	0.26 × 0.34
[24]	1.39/1.83	9.3/6.6	2.48/3.6	2	N.A.
[25]	2.3/4.1	N.A.	0.65/1	3	0.39 × 0.39
[26]	1.91/2.62	2.39/2.29	0.29/0.45	4	0.39 × 0.156
[28]	2.4/5.2	8/5	1.6/2.2	5	0.26 × 0.22
This work	**2.4/5.2**	**10.6/13.5**	**0.36/1.0**	**6**	**0.10 × 0.11**

* Filter based on Superconductor material

same with the independent ones. Moreover, the selectivity of both the first and second passbands are improved, and the rejection levels of lower and upper stopband are also enhanced. Besides, the isolation between the two passbands is enlarged simultaneously.

As a demonstration, a dual-band BPF, as shown in Fig. 1(a), is designed, fabricated and measured. The simulated two passbands are centered at 2.4 and 5.2 GHz, respectively. The final optimized dimensions of the dual-band BPF demonstrated in Fig. 1(a) are as follows: $W_1 = 0.8$ mm, $W_2 = 0.3$ mm, $W_3 = 0.15$ mm, $W_4 = 0.15$ mm, $W_5 = 0.15$ mm, $W_{s1} = 0.6$ mm, $W_{s2} = 1.3$ mm, $L_1 = 6.55$ mm, $L_2 = 7.11$ mm, $L_3 = 8.14$ mm, $L_4 = 9.78$ mm, $L_5 = 0.8$ mm, $L_{s1} = 0.85$ mm, $L_{s2} = 0.79$ mm, $g = 0.1$ mm, $g_1 = 0.15$ mm, $s = 0.12$ mm, $D = 0.58$ mm, $d = 3.18$ mm.

Fig. 11(a) shows the photograph of the fabricated dual-band BPF. The simulation and measurement are accomplished by using Ansys HFSS and Agilent N5244A vector network analyzer, respectively. The comparison between the simulated and measured results are shown in Fig. 11 (b). The measured two passbands are centered at

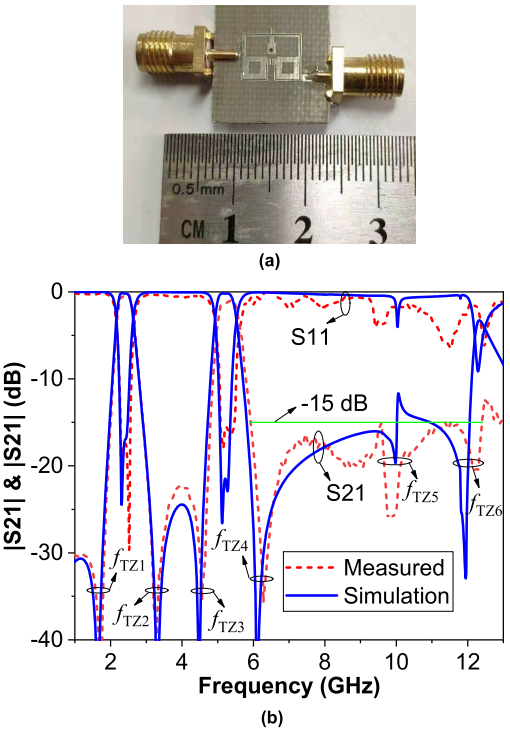

FIGURE 11. Photograph and measurement of fabricated dual-band BPF, (a) photograph, (b) comparison of measured and simulated results.

2.4 and 5.2 GHz with the fractional bandwidths of 10.6 and 13.5%. The measured in-band return losses are better than 17.4 and 15.8 dB and the insertion losses are less than 0.36 and 1 dB, respectively. Six transmission zeros are distributed at 1.65, 3.3, 4.45, 6.15, 9.96 and 11.95 GHz which improve the selectivity and isolation between each passband. It is worth mentioning that there is a broad upper stopband ranging from 5.81 to 12.41 GHz with −15 dB rejection. The measured results are in good agreement with the simulated ones. Slight deviation is observed, which could be attributed to fabrication tolerance in the implementation. Stepped impedance and folding had been employed to achieve compactness and the overall filter size amounted to 7.74 mm × 8.54 mm, which occupies only 0.10 $\lambda_g \times$ 0.11 λ_g, where λ_g is the guided wavelength at the center frequency of the first passband. A performance comparison between the reported dual-band BPFs and the proposed one is shown in Table 1. It shows that the proposed dual-band BPF has the advantages of low insertion loss (*IL*), wide passband, high selectivity, compact size and simple circuit topology.

V. CONCLUSION

A compact dual-band BPF, which is the combination of Filter I and II, based on the RLR and 0° feed structure, is presented in this paper. For Filter I, the theoretical and numerical studies on RLR are implemented firstly, and then the RLR based BPF is designed. Based on the 0° feed structure, a novel feed structure is proposed to from the Filter II with high selectivity. By combining the aforementioned Filter I and II, a compact dual-band BPF with good selectivity is obtained with the

circuit size no increased. Finally, a demonstrated dual-band BPF is designed, fabricated and measured. The measured results agree well with the simulated ones. The comparison between the some reported dual-band BPF, the proposed one has the advantages of low insertion loss, wide passband, high selectivity, compact size and simple circuit topology.

REFERENCES

[1] D. Li, J.-A. Wang, Z. Chen, Y. Zhang, M.-C. Tang, and L. Yang, "Compact microstrip bandpass filter with sharp roll-off and broad stopband using modified 0° feed structure," *AEU-Int. J. Electron. Commun.*, vol. 109, pp. 17–22, Sep. 2019.
[2] J. Xu and Y. Zhu, "Tunable bandpass filter using a switched tunable diplexer technique," *IEEE Trans. Ind. Electron.*, vol. 64, no. 4, pp. 3118–3126, Apr. 2017.
[3] D. Li, Y. Zhang, X. Feng, K. Song, Y. Fan, J. Xie, and Y. Liao, "Multichannel radiometer frontend based on bandwidth synthetic technology," *IEEE Trans. Microw. Theory Techn.*, vol. 65, no. 2, pp. 632–640, Feb. 2017.
[4] X. Y. Zhang, C. H. Chan, Q. Xue, and B.-J. Hu, "RF tunable bandstop filters with constant bandwidth based on a doublet configuration," *IEEE Trans. Ind. Electron.*, vol. 59, no. 2, pp. 1257–1265, Feb. 2012.
[5] D. Li, J. Wang, Y. Liu, Z. Chen, and L. Yang, "Compact quasi-elliptic bandpass filter with high selectivity using short-circuited coupled line," *Microw. Opt. Technol. Lett.*, vol. 61, no. 12, pp. 2873–2878, Dec. 2019.
[6] Z. Wang, J. R. Kelly, P. S. Hall, A. L. Borja, and P. Gardner, "Reconfigurable parallel coupled band notch resonator with wide tuning range," *IEEE Trans. Ind. Electron.*, vol. 61, no. 11, pp. 6316–6326, Nov. 2014.
[7] K. Ma, R. M. Jayasuriya, and D. R. Lim Chin Siong, "Fully integrated high-isolation low-loss digitally controlled MEMS filters," *IEEE Trans. Ind. Electron.*, vol. 58, no. 7, pp. 2690–2696, Jul. 2011.
[8] J.-X. Chen, Y. Ma, J. Cai, L.-H. Zhou, Z.-H. Bao, and W. Che, "Novel frequency-agile bandpass filter with wide tuning range and spurious suppression," *IEEE Trans. Ind. Electron.*, vol. 62, no. 10, pp. 6428–6435, Oct. 2015.
[9] H.-W. Liu, Y.-F. Lv, and W. Zheng, "Compact dual-band bandpass filter using trisection hairpin resonator for GPS and WLAN applications," *Electron. Lett.*, vol. 45, no. 7, p. 360, 2009.
[10] Y. Mo, Y. Fan, P. Tao, and K. Song, "Miniaturised dual-band bandpass filter using modified SIR," *Electron. Lett.*, vol. 49, no. 14, pp. 888–890, Jul. 2013.
[11] A. Genc, R. Baktur, and R. J. Jost, "Dual-bandpass filters with individually controllable passbands," *IEEE Trans. Compon., Packag., Manuf. Technol.*, vol. 3, no. 1, pp. 105–112, Jan. 2013.
[12] D. Li, Y. Zhang, K. Xu, K. Song, and L.-W. Li, "Compact dual-wideband bandpass filter with good selectivity using side-coupled λ/4 shorted SIR," *J. Electromagn. Waves Appl.*, vol. 29, no. 1, pp. 69–79, Jan. 2015.
[13] M.-L. Chuang, M.-T. Wu, and S.-M. Tsai, "Dual-band filter design using L shaped stepped impedance resonators," *IET Microw., Antennas Propag.*, vol. 4, no. 7, pp. 855–862, Jul. 2010.
[14] W. Jiang, W. Shen, T. Wang, Y. M. Huang, Y. Peng, and G. Wang, "Compact dual-band filter using open/short stub loaded stepped impedance resonators (OSLSIRs/SSLSIRs)," *IEEE Microw. Wireless Compon. Lett.*, vol. 26, no. 9, pp. 672–674, Sep. 2016.
[15] Z.-C. Zhang, Q.-X. Chu, and F.-C. Chen, "Compact dual-band bandpass filters using open-/short-circuited stub-loaded λ/4 resonators," *IEEE Microw. Wireless Compon. Lett.*, vol. 25, no. 10, pp. 657–659, Oct. 2015.
[16] X. Y. Zhang, J.-X. Chen, Q. Xue, and S.-M. Li, "Dual-band bandpass filters using stub-loaded resonators," *IEEE Microw. Wireless Compon. Lett.*, vol. 17, no. 8, pp. 583–585, Aug. 2007.
[17] L. Gao and X. Y. Zhang, "High-selectivity dual-band bandpass filter using a quad-mode resonator with source-load coupling," *IEEE Microw. Wireless Compon. Lett.*, vol. 23, no. 9, pp. 474–476, Sep. 2013.
[18] L. Gao, X. Y. Zhang, B.-J. Hu, and Q. Xue, "Novel multi-stub loaded resonators and their applications to various bandpass filters," *IEEE Trans. Microw. Theory Techn.*, vol. 62, no. 5, pp. 1162–1172, May 2014.
[19] Q.-X. Chu and F.-C. Chen, "A compact dual-band bandpass filter using meandering stepped impedance resonators," *IEEE Microw. Wireless Compon. Lett.*, vol. 18, no. 5, pp. 320–322, May 2008.
[20] F. Song, B. Wei, L. Zhu, B. Cao, and X. Lu, "Dual-band high-temperature superconducting bandpass filter using quint-mode stub-loaded resonators," *IEEE Trans. Appl. Supercond.*, vol. 25, no. 4, pp. 1–10, Aug. 2015.
[21] T.-H. Huang, H.-J. Chen, C.-S. Chang, L.-S. Chen, Y.-H. Wang, and M.-P. Houng, "A novel compact ring dual-mode filter with adjustable second-passband for dual-band applications," *IEEE Microw. Wireless Compon. Lett.*, vol. 16, no. 6, pp. 360–362, Jun. 2006.
[22] S. Luo, L. Zhu, and S. Sun, "A dual-band ring-resonator bandpass filter based on two pairs of degenerate modes," *IEEE Trans. Microw. Theory Techn.*, vol. 58, no. 12, pp. 3427–3432, Dec. 2010.
[23] B. Ren, H. Liu, Z. Ma, M. Ohira, P. Wen, X. Wang, and X. Guan, "Compact dual-band differential bandpass filter using quadruple-mode stepped-impedance square ring loaded resonators," *IEEE Access*, vol. 6, pp. 21850–21858, 2018.
[24] J. Shi, L. Lin, J. Chen, H. Chu, and X. Wu, "Dual-band bandpass filter with wide stopband using one stepped-impedance ring resonator with shorted stubs," *IEEE Microw. Wireless Compon. Lett.*, vol. 24, no. 7, pp. 442–444, Jul. 2014.
[25] S. Sun, "A dual-band bandpass filter using a single dual-mode ring resonator," *IEEE Microw. Wireless Compon. Lett.*, vol. 21, no. 6, pp. 298–300, Jun. 2011.
[26] H. Liu, B. Ren, S. Hu, X. Guan, P. Wen, and J. Tang, "High-order dual-band superconducting bandpass filter with controllable bandwidths and multitransmission zeros," *IEEE Trans. Microw. Theory Techn.*, vol. 65, no. 10, pp. 3813–3823, Oct. 2017.
[27] M. Zhou, X. Tang, and F. Xiao, "Compact dual band bandpass filter using novel E-type resonators with controllable bandwidths," *IEEE Microw. Wireless Compon. Lett.*, vol. 18, no. 12, pp. 779–781, Dec. 2008.
[28] M. Zhou, X. Tang, and F. Xiao, "Compact dual band transversal bandpass filter with multiple transmission zeros and controllable bandwidths," *IEEE Microw. Wireless Compon. Lett.*, vol. 19, no. 6, pp. 347–349, Jun. 2009.
[29] K. Chang and L.-H. Hsieh, *Microwave Ring Circuits and Related Structures*. Hoboken, NJ, USA: Wiley, 2004.
[30] C.-C. Yu and K. Chang, "Transmission-line analysis of a capacitively coupled microstrip-ring resonator," *IEEE Trans. Microw. Theory Techn.*, vol. 45, no. 11, pp. 2018–2024, Nov. 1997.
[31] D. M. Pozar, *Microwave Engineering*. Hoboken, NJ, USA: Wiley, 2009.
[32] X. Yin Zhang, J. Shi, J.-X. Chen, and Q. Xue, "Dual-band bandpass filter design using a novel feed scheme," *IEEE Microw. Wireless Compon. Lett.*, vol. 19, no. 6, pp. 350–352, Jun. 2009.
[33] S. Zhang and L. Zhu, "Synthesis method for even-order symmetrical Chebyshev bandpass filters with alternative J/K inverters and λ/4 resonators," *IEEE Trans. Microw. Theory Techn.*, vol. 61, no. 2, pp. 808–816, Feb. 2013.
[34] S.-C. Lin, "Microstrip dual/quad-band filters with coupled lines and quasi-lumped impedance inverters based on parallel-path transmission," *IEEE Trans. Microw. Theory Techn.*, vol. 59, no. 8, pp. 1937–1946, Aug. 2011.
[35] T. Edwards, *Foundations for Microstrip Circuit Design*, 2nd ed. New York, NY, USA: Wiley, 1992.
[36] C.-M. Tsai, S.-Y. Lee, and C.-C. Tsai, "Performance of a planar filter using a 0° feed structure," *IEEE Trans. Microw. Theory Techn.*, vol. 50, no. 10, pp. 2362–2367, Oct. 2002.

DAOTONG LI (Member, IEEE) received the Ph.D. degree in electromagnetic field and microwave technology from the University of Electronic Science and Technology of China (UESTC), Chengdu, China, in 2016.

He is currently with the Center of Communication and Tracking Telemetry Command, Chongqing University, Chongqing. Since 2015, he has been a Visiting Researcher with the Department of Electrical and Computer Engineering, University of Illinois at Urbana–Champaign, Urbana, IL, USA, with financial support from the China Scholarship Council. He has authored or coauthored over 70 peer-reviewed journal or conference papers. His current research interests include RF, microwave and millimeter-wave technology and applications, microwave power transmission (MPT), antennas, devices, circuits and systems, and passive and active (sub-) millimeter-wave imaging, and radiometer.

Dr. Li was a recipient of the UESTC Outstanding Graduate Awards by the Sichuan province and UESTC, in 2016. He was also a recipient of the National Graduate Student Scholarship from the Ministry of Education, China, and Tang Lixin Scholarship. He is serving as a reviewer for the several IEEE and IET journals, and many international conferences as a TPC member, a Session Organizer, and the Session Chair.

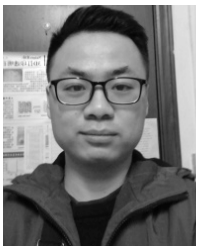

JU-AN WANG was born in Wuhan, Hubei, China, in 1996. He received the B.E. degree in electronic information engineering from HUBU, Wuhan, in 2018. He is currently pursuing the M.E. degree in electromagnetic fields and microwave technology with Chongqing University, Chongqing, China.

His research interests include the characterization and development of RF and microwave components, circuits, antennas, filter, and metamaterials.

YING LIU received the B.E. degree in communications engineering from the Qingdao University of Science and Technology, Qingdao, China, in 2012, and the M.S. degree in communication and information system from Chongqing University, Chongqing, in 2015.

She is currently with the School of Microelectronics and Communication Engineering, Chongqing University. Her current research interests include microwave and optical image processing, microwave photonics, and microwave and millimeter wave circuit and systems.

ZHEN CHEN was born in Zigong, Sichuan, China, in 1995. He received the B.E. degree in communication engineering from CDUT, Chengdu, China, in 2018. He is currently pursuing the M.E. degree in electromagnetic fields and microwave technology with Chongqing University, Chongqing, China.

His current research interests include the filtering patch antenna and rectifier circuit in microwave power transmission.